Thermal relaxation in young neutron stars

Oleg Y. Gnedin,[1]* Dmitry G. Yakovlev[1,3] and Alexander Y. Potekhin[2]

[1]*Institute of Astronomy, Madingley Road, Cambridge CB3 0HA*
[2]*Ioffe Physical Technical Institute, 194021, St Petersburg, Russia*
[3]*Institute for Theoretical Physics, University of California, Santa Barbara, CA 93106, USA*

ABSTRACT

The internal properties of the neutron star crust can be probed by observing the epoch of thermal relaxation. After the supernova explosion, powerful neutrino emission quickly cools the stellar core, while the crust stays hot. The cooling wave then propagates through the crust, as a result of its finite thermal conductivity. When the cooling wave reaches the surface (age 10–100 yr), the effective temperature drops sharply from 250 eV to 30 or 100 eV, depending on the cooling model. The crust relaxation time is sensitive to the (poorly known) microscopic properties of matter of subnuclear density, such as the heat capacity, thermal conductivity, and superfluidity of free neutrons. We calculate the cooling models with the new values of the electron thermal conductivity in the inner crust, based on a realistic treatment of the shapes of atomic nuclei. Superfluid effects may shorten the relaxation time by a factor of 4. The comparison of theoretical cooling curves with observations provides a potentially powerful method of studying the properties of the neutron superfluid and highly unusual atomic nuclei in the inner crust.

Key words: dense matter – stars: neutron – X-rays: stars.

1 INTRODUCTION

Neutron stars are natural astrophysical laboratories of superdense matter. In their cores, at densities above the nuclear matter density $\rho_0 = 2.8 \times 10^{14}\,\text{g cm}^{-3}$, the properties of matter, such as equation of state and even composition, are largely unknown (e.g. Lattimer & Prakash 2000, and references therein). In the absence of an exact theory of superdense matter, different theoretical models predict different equations of state and compositions (neutrons, protons and electrons; hyperons; pion or kaon condensates; deconfined quarks).

One of the potentially powerful methods used to probe the internal structure of isolated neutron stars is modelling their cooling (e.g. Pethick 1992; Page & Applegate 1992; Page 1998a,b). The theoretical cooling curves depend on the adopted physical models of the stellar interior, especially the neutrino emission and heat capacity, as well as the superfluidity of neutrons and protons in the core. Confronting theory and observations allows one, for example, to constrain the range of the critical temperatures of the superfluidity (e.g. Yakovlev et al. 1999).

Observing the thermal emission of the very young neutron stars, with $t \lesssim 100$ yr, opens a possibility of studying the properties of the neutron star crust. Soon after a supernova explosion, the young star has large temperature gradients in the inner parts of the crust. While the powerful neutrino emission quickly cools the core, the crust stays hot. The heat gradually flows inward on a conduction time-scale, and the whole process can be thought of as a cooling wave propagation from the centre towards the surface. During this thermal relaxation the effective temperature stays almost constant at about 250 eV. When the cooling wave reaches the surface, the effective temperature drops sharply by as much as an order of magnitude in the fast-cooling scenario, and by a factor of 2–3 in the slow-cooling scenario. The duration of the relaxation epoch depends mainly on the heat capacity and the thermal conductivity of the inner crust (Lattimer et al. 1994).

Although the equation of state of matter at subnuclear density is known accurately enough (Negele & Vautherin 1973; Pethick & Ravenhall 1995), the properties of atomic nuclei are not. The nuclei become unusually neutron-rich, with the smooth proton and neutron distributions. At the bottom of the crust ($\rho \gtrsim 10^{14}\,\text{g cm}^{-3}$), the nuclei can be non-spherical and form clusters (Lorenz, Ravenhall & Pethick 1993; Pethick & Ravenhall 1995). The liquid of neutrons dripped from the nuclei may be superfluid, with critical temperatures that are very model-dependent. The thermodynamic and transport properties of this matter are subjects of large theoretical uncertainty.

In this paper we make improved models of the young neutron stars. We obtain the new values of the electron thermal conductivity in the inner crust, based on a realistic treatment of the shapes of atomic nuclei. Using a new numerical code, we calculate the cooling models and determine the duration of the thermal relaxation epoch. We extend the analysis of Lattimer et al.

(1994) and derive the dependence of the relaxation time on the microscopic parameters of the crust. Our preliminary results have been summarized by Yakovlev et al. (2001a).

2 COOLING MODEL

2.1 Equations of thermal evolution

Neutron stars are born very hot in supernova explosions, with the internal temperature $T \sim 10^{11}$ K, but gradually cool down. About 20 s after birth, they become fully transparent for the neutrinos generated in numerous reactions in stellar interiors. We consider the cooling in the following neutrino-transparent stage. The cooling is realized via two channels, by neutrino emission from the entire stellar body and by heat conduction from the internal layers to the surface resulting in thermal emission of photons. For simplicity, we neglect the possible reheating mechanisms (frictional dissipation of the rotational energy, Ohmic decay of the internal magnetic field, or the dissipation associated with weak deviations from the chemical equilibrium; see, e.g., Page 1998a).

The internal structure of neutron stars can be regarded as temperature-independent (e.g. Shapiro & Teukolsky 1983). The relativistic equations of thermal evolution include the energy and flux equations (Thorne 1977):

$$\frac{1}{4\pi r^2 e^{2\Phi}}\sqrt{1-\frac{2Gm}{c^2 r}}\frac{\partial}{\partial r}(e^{2\Phi}L_r) = -Q_\nu - \frac{C_v}{e^{\Phi}}\frac{\partial T}{\partial t}, \qquad (1)$$

$$\frac{L_r}{4\pi r^2} = -\kappa\sqrt{1-\frac{2Gm}{c^2 r}}\,e^{-\Phi}\frac{\partial}{\partial r}(Te^{\Phi}), \qquad (2)$$

where Q_ν is the neutrino emissivity (erg cm^{-3} s^{-1}), C_v is the specific heat capacity (erg cm^{-3} K^{-1}), κ is the thermal conductivity and L_r is the 'local luminosity', defined as the non-neutrino heat flux transported through a sphere of radius r. The gravitational mass $m(r)$ and the metric function $\Phi(r)$ are determined by the stellar model. After thermal relaxation, the redshifted temperature $\tilde{T}(t) \equiv T(r,t)e^{\Phi(r)}$ becomes constant throughout the interior.

It is conventional (Gudmundsson, Pethick & Epstein 1983) to subdivide the calculation of heat transport in the neutron star interior ($r < R_b$) and in the outer heat-blanketing envelope ($R_b \leq r \leq R$), where R is the stellar radius, and the boundary radius R_b corresponds to the density $\rho_b = 10^{10}$ g cm^{-3} (~ 100 m under the surface). The thermal structure of the blanketing envelope is studied separately in the stationary, plane-parallel approximations in order to relate the effective surface temperature T_s to the temperature at the inner boundary of the envelope T_b. We use the T_s–T_b relation obtained by Potekhin, Chabrier & Yakovlev (1997) for the envelope, which is composed mostly of iron.

The effective temperature determines the photon luminosity; $L_\gamma = L_r(R,t) = 4\pi\sigma R^2 T_s^4(t)$. Both L_γ and T_s refer to the locally flat reference frame on the surface. A distant observer would register the 'apparent' luminosity as $L_\gamma^\infty = L_\gamma(1 - r_g/R)$ and the 'apparent' effective temperature as $T_s^\infty = T_s\sqrt{1 - r_g/R}$, where $r_g = 2GM/c^2$ is the gravitational radius. Typically, $r_g/R = 30$–40 per cent.

We have developed a new evolutionary code based on the Henyey-type scheme on a grid of spherical shells (Kippenhahn, Weigert & Hofmeister 1967). The hydrostatic model of the neutron star with a given equation of state is calculated separately and is fixed throughout the calculation. In the initial configuration the star has a constant redshifted temperature throughout the interior, $\tilde{T} = 10^{10}$ K, and no heat flux, $L_r = 0$. Also, to improve numerical

convergence, the thermal conductivity in the core is boosted for the initial epoch $t < 10^{-2}$ yr. As the crust is thermally detached from the core at such a small age, this correction has no effect on the cooling curves. Full details of the new code are available on the Internet (http://www.ast.cam.ac.uk/~ognedin/ns/ns.html).

2.2 Physics input

We use the equation of state of Negele & Vautherin (1973) in the stellar crust with the smooth composition model of ground-state matter to describe the properties of atomic nuclei (Kaminker et al. 1999). We assume that the nuclei are spherical throughout the entire crust. The core–crust interface is placed at $\rho_{cc} = 1.5 \times 10^{14}$ g cm^{-3}. For simplicity, we consider the neutron star cores to be composed of neutrons (n), protons (p) and electrons (e) and use the moderately stiff phenomenological equation of state of Prakash, Ainsworth & Lattimer (1988) (in the simplified version proposed by Page & Applegate 1992), in agreement with our previous work (Yakovlev et al. 1999 and references therein).

The parameters of the models are summarized in Table 1. It shows the stellar masses, radii, central densities, crust masses and crust thicknesses for a number of models. The maximum mass of the stable neutron stars with this equation of state is 1.73 M$_\odot$. We define the crust thickness as $\Delta R_{crust} = R - R_{core}$, while the proper geometrical thickness (for $\Delta R_{crust} \ll R$) is $\Delta R_{crust}/\sqrt{1 - r_g/R}$. As we increase the mass M, the radii and crust masses of the stable configurations get smaller, i.e. the stars become more compact.

Free neutrons in the inner crust and both neutrons and protons in the core of a neutron star are likely to be superfluid. We assume the singlet-state pairing of the protons in the core. The superfluidity of the free neutrons in the crust and of the neutrons in the outermost part of the core is known to be of the singlet-state type, but at higher densities it switches to the triplet-state type. Various microscopic theories predict a large scatter of the critical temperatures of the neutron and proton superfluids, T_{cn} and T_{cp}, depending on the nucleon–nucleon potential model and the many-body theory employed (see Yakovlev et al. 1999 for references).

As an example we will use two models, a *weak* and a *strong* superfluidity (Fig. 1). The model of strong superfluidity corresponds to the higher T_c. It is based on the rather large energy gaps calculated by Elgarøy et al. (1996) for the singlet-state pairing (with the maximum gap of about 2.5 MeV) and by Hoffberg et al. (1970) for the triplet-state pairing. The weak superfluid model makes use of the smaller gaps derived by Wambach, Ainsworth &

Table 1. Neutron star models.

M (M$_\odot$)	R (km)	ρ_{c14}[c]	M_{crust} (M$_\odot$)	ΔR_{crust}[d] (km)	M_D (M$_\odot$)	R_D (km)
1.1	12.20	8.50	0.050	1.66	…	…
1.2	12.04	9.52	0.044	1.45	…	…
1.3	11.86	10.70	0.039	1.26	…	…
1.4	11.65	12.20	0.033	1.09	…	…
1.44[a]	11.54	12.98	0.031	1.02	0.000	0.00
1.5	11.38	14.20	0.028	0.93	0.065	2.84
1.6	11.01	17.20	0.022	0.77	0.301	4.61
1.7	10.37	23.50	0.016	0.59	0.685	5.79
1.73[b]	9.71	32.50	0.011	0.47	0.966	6.18

[a] Threshold configuration for switching on direct Urca process.
[b] Configuration with maximum allowable mass.
[c] Central density in 10^{14} g cm^{-3}.
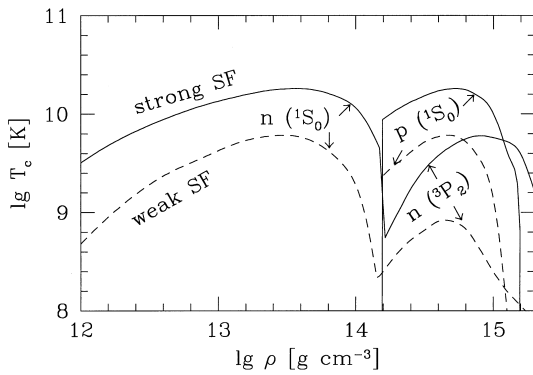[d] ΔR_{crust} is defined as $R - R_{core}$.

Figure 1. Density dependence of the critical temperatures of superfluidity (SF) of free neutrons in the inner crust, and neutrons and protons in the core for the strong (solid lines) and weak (dashed lines) superfluid models (see text for details).

Pines (1993) (with the maximum gap of about 1 MeV) for the singlet-state superfluid and by Amundsen & Østgaard (1985) for the triplet-state neutron superfluid. For simplicity, we use the same function $T_c(n)$ to describe the singlet pairing of free neutrons in the crust ($n = n_n$) and of the protons in the core ($n = n_p$).

The cooling of neutron stars is mainly determined by the neutrino emissivity, specific heat capacity and thermal conductivity. We include all the relevant sources of neutrino emission (Yakovlev et al. 1999, 2001b): the direct and modified Urca processes, nn, pp and np bremsstrahlung in the core; and plasmon decay, e^-e^+ pair annihilation, electron–nucleus (eZ) and nn bremsstrahlung in the crust. The emissivity of the proton branch of the modified Urca process derived by Yakovlev & Levenfish (1995) has been corrected by Yakovlev et al. (2001), which has almost no effect on the cooling curves. We include the proper reduction of the neutrino reactions by superfluidity and also an additional neutrino emission that is a result of Cooper pairing of superfluid nucleons. The effective nucleon masses in the core and the crust are set equal to 0.7 of their bare masses.

A very important cooling effect is produced by the powerful direct Urca process (Lattimer et al. 1991). For our equation of state, this process is allowed at densities above the threshold, $\rho_{\rm crit} = 1.298 \times 10^{15}\,{\rm g\,cm^{-3}}$. If the central density of the model exceeds the threshold, $\rho_c > \rho_{\rm crit}$, the stellar core has a central kernel where the direct Urca process leads to fast cooling. The masses and radii of these kernels, $M_{\rm D}$ and $R_{\rm D}$, are given in Table 1. The mass of the central kernel increases rapidly with M. In addition, we show the threshold configuration with $\rho_c = \rho_{\rm crit}$. It separates the low-mass models, where the direct Urca process is forbidden, from the high-mass models, where the direct Urca is allowed.

For illustration, Fig. 2 shows the emissivity of various neutrino processes versus density at $T = 10^9\,{\rm K}$. The plasmon decay is a powerful neutrino emission mechanism in a hot crust at not very high densities, but it fades away quickly when the temperature decreases below $10^9\,{\rm K}$. The electron–nucleus bremsstrahlung is efficient throughout the entire crust. In superfluid crusts, the Cooper pairing neutrino emission switches on at temperatures $T = T_{\rm cn}$, reaches maximum at T slightly below $T_{\rm cn}$, and fades away exponentially for $T \ll T_{\rm cn}$. In the neutron star core, a large jump of the neutrino emissivity at $\rho = \rho_{\rm crit}$ is associated with the direct Urca process.

The heat capacity is contributed to by neutrons, protons and electrons in the core, and by electrons, free neutrons and atomic
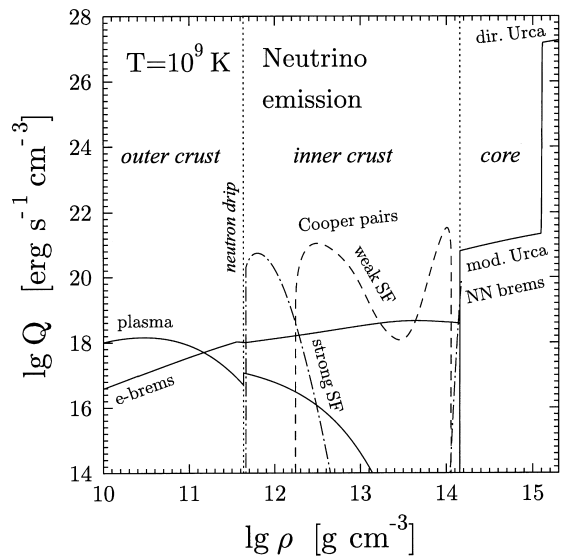

Figure 2. Density dependence of the neutrino emissivity at $T = 10^9\,{\rm K}$. Solid lines: partial emissivities due to electron–nucleus bremsstrahlung (e-brems) and plasmon decay (plasma) in the crust and the total emissivity produced by direct and modified Urca processes and by nucleon-nucleon (*NN*) bremsstrahlung in the nonsuperfluid core. Dashed and dash-dot lines: the emissivity due to Cooper pairing of neutrons for the models of strong and weak superfluidity in the crust. Vertical dotted lines indicate the neutron drip density and the boundary of the core.
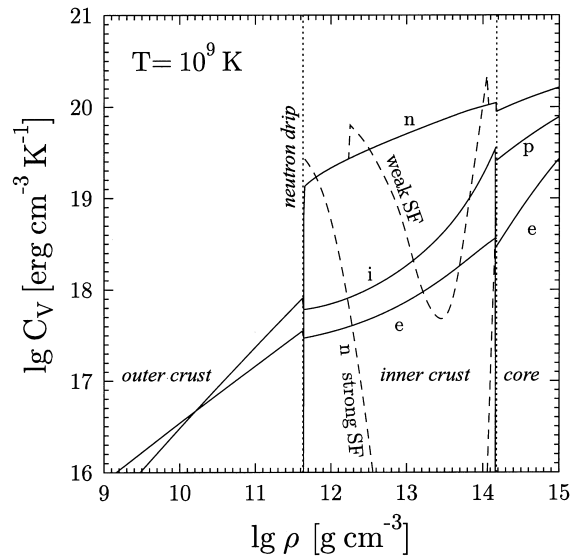

Figure 3. Density dependence of the specific heat capacity at $T = 10^9\,{\rm K}$. Solid lines: partial heat capacities of ions (i), electrons (e) and free neutrons (n) in non-superfluid crusts, as well as of neutrons, protons (p) and electrons in nonsuperfluid cores. Dashed lines: heat capacities of free neutrons in the crust modified by weak or strong superfluidity.

nuclei (vibrations of ions in Coulomb lattice) in the crust. The superfluid effects on the heat capacity of nucleons in the core and of free neutrons in the crust are incorporated according to Levenfish & Yakovlev (1994). In the absence of superfluidity, the neutrons would have the dominant contribution in the core and the inner crust. The effects of neutron superfluidity are illustrated in Fig. 3 in the case of crust superfluidity. When T falls only slightly below $T_{\rm cn}$, the superfluidity increases the neutron heat capacity caused by the latent heat released at the phase transition. However,
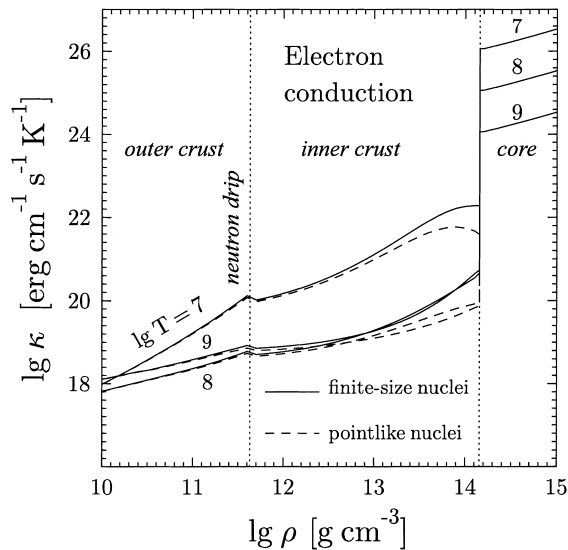
Figure 4. Density dependence of the electron thermal conductivity at $T = 10^7$, 10^8 and 10^9 K in the core and the crust.

Figure 5. Cooling curves for non-superfluid neutron star models with 1.1, 1.2 …, 1.7 M$_\odot$.

for $T \ll T_{cn}$ the superfluidity exponentially reduces the heat capacity. If the stellar crust was sufficiently colder than in Fig. 3, any neutron superfluid would reduce the contribution of free neutrons to negligibly small values, and the heat capacity would be determined by the ions and electrons. These effects are analogous in the core. The heat capacity in the superfluid core at $T \ll T_{cn}$ and $T \ll T_{cp}$ would be determined by the electrons.

The thermal conductivity in the core is taken as a sum of the conductivities of the electrons (Gnedin & Yakovlev 1995) and neutrons (Baiko, Haensel & Yakovlev 2001). The electron contribution usually dominates. The conductivity in the crust is assumed to be as a result of the electron scattering off atomic nuclei. In the outer crust the finite size of the proton charge distribution within a nucleus can be neglected. We use the recent results of Potekhin et al. (1999), which include the multiphonon processes in electron–nucleus scattering in a Coulomb solid and incipient long-range nucleus–nucleus correlations in a strongly coupled Coulomb liquid of atomic nuclei. In the inner crust, we have performed original calculations using the same formalism but have taken into account the finite size of the proton core of atomic nuclei (finite-size nuclei). Details of the calculations and the numerical fits are given in the Appendix.

The results are illustrated in Fig. 4, which shows the density profiles of the electron thermal conductivity for $T = 10^7$, 10^8 and 10^9 K. The conductivity in the core is several orders of magnitude higher than in the crust, because there are not as efficient electron scatterers in the core as atomic nuclei. In the crust we plot the thermal conductivity for finite-size nuclei (solid lines) and for point-like nuclei (dashed lines). The finite-size effects are negligible near the neutron drip point but increase the conductivity at the crust base ($\rho \sim 10^{14}$ g cm^{-3}) by a factor of 3–5.

Another contribution to the thermal conductivity in the crust may come from the scattering of electrons off charged impurities, which are the randomly distributed nuclei of different elements. However, the most important temperature interval for neutron star cooling is $\sim 10^8$–10^9 K. We have verified that the thermal conductivity is almost unaffected by the impurities in this temperature interval (for a not very impure matter, $Q_{imp} \lesssim 1$, where Q_{imp} is the impurity parameter as defined in the Appendix), although they can noticeably decrease the conductivity at lower T.
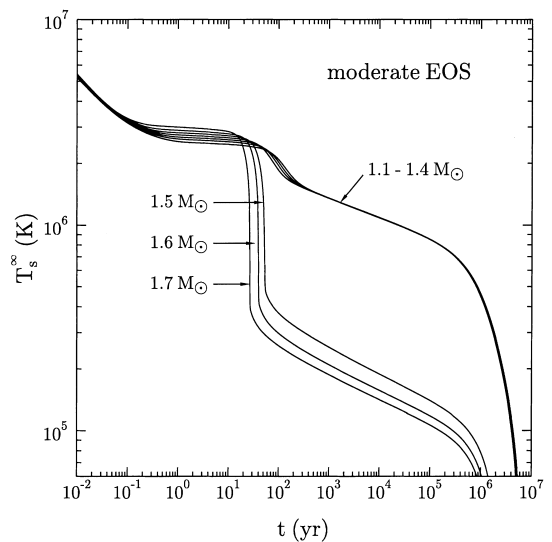
Therefore, we neglect the effects of impurities in the present calculations.

3   THERMAL RELAXATION IN NON-SUPERFLUID NEUTRON STARS

First, consider thermal relaxation in a young non-superfluid neutron star. The main features of the process are known from previous cooling simulations (Page & Applegate 1992; Lattimer et al. 1994; Page 1998a,b; and references therein).

Fig. 5 shows some cooling models of neutron stars with different masses. In the low-mass models, $M < 1.44$ M$_\odot$, the direct Urca process is forbidden. These stars follow the standard cooling scenario and the cooling curves are almost independent of M. The high-mass models go through the fast-cooling scenario and demonstrate a spectacular drop in surface temperature at the end of the thermal relaxation epoch, $t \sim 50$ yr, as a result of the emergence of the cooling wave on the surface. The same, although much less pronounced, effect takes place in the case of slow cooling.

As the neutrino emissivity of the direct Urca process is several orders of magnitude larger than that of the modified Urca processes, the fast-cooling regime is established even if the central kernel, where the direct Urca process is allowed, occupies a small fraction of the stellar core (Page & Applegate 1992). For the high-mass stars ($M > 1.44$ M$_\odot$), the cooling curves again depend weakly on the mass. The change of the slope of the cooling curves at $t \sim 10^5$–10^6 yr manifests the transition from the neutrino to the photon cooling stage.

The surface temperature at the initial cooling stage (the first 100 years) is rather independent of the equation of state, the stellar mass or the core neutrino luminosity. The surface temperature is mainly determined by the physical properties of matter in the crust. The core and the crust are thermally decoupled, and the effective surface temperature does not reflect the thermal state of the stellar core.

In contrast, the evolution of the central temperature, $T(0,t)$, is drastically different for the slow- and fast-cooling scenarios. In all low-mass models, $T(0,t) \propto t^{-1/6}$ throughout the neutrino cooling era, $t \lesssim 10^5$ yr, with a small offset in normalization. This follows

from the simple power-law temperature dependence of the heat capacity ($C_v \propto T$) and the standard neutrino emissivity ($Q_\nu \propto T^8$). In the models with fast cooling, where the dominant neutrino process is the direct Urca ($Q_\nu \propto T^6$), the scaling relation is $T(0, t) \propto t^{-1/4}$ for the initial period $t < 10^{-2}$ yr. However, until $t \lesssim 10$ yr the central temperature remains almost constant at 10^8 K as the heat flows from the warmer outer core, in which direct Urca process is prohibited, into the inner core. During the thermal relaxation epoch, $10 < t < 100$ yr, the central temperature falls again by a factor of several. After the thermalization until the end of the neutrino era, once again $T(0, t) \propto t^{-1/4}$.

Figs 6 and 7 illustrate the effects of thermal relaxation on the internal temperature profiles in the slow- and fast-cooling scenarios, respectively. Until the age of about 1 yr, the neutron star core and the inner and outer crusts form almost independent
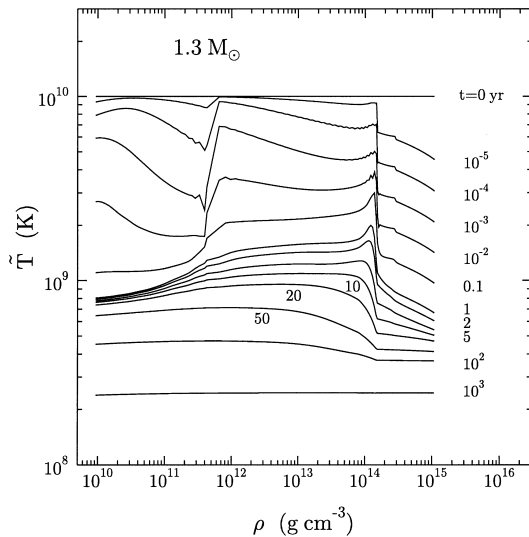

Figure 6. Temperature profiles in the 1.3-$M_\odot$ neutron star without superfluid effects. The numbers next to the curves show stellar age. Contours are at 0, 10^{-5}, 10^{-4}, 10^{-3}, 10^{-2}, 10^{-1}, 1, 2, 5, 10, 20, 50, 100 and 1000 yr.
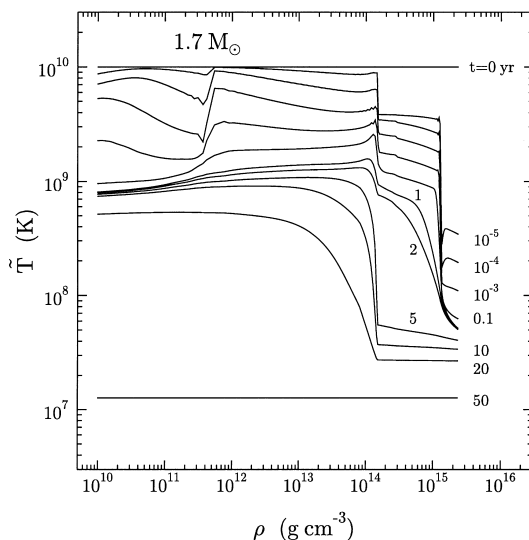

Figure 7. Temperature profiles in the 1.7-$M_\odot$ neutron star without superfluid effects. The contours are at 0, 10^{-5}, 10^{-4}, 10^{-3}, 10^{-2}, 10^{-1}, 1, 2, 5, 10, 20 and 50 yr.

thermal reservoirs. The region around 4×10^{11} g cm^{-3}, where free neutrons appear in the crust, seems to be the most effective at cooling, owing to the powerful neutrino emission (see below). The outer crust cools to 10^9 K in less than a month, while the inner parts remain much hotter. The core also cools independently but is unable to affect the inner crust because of the slow thermal conduction. During the first years the central kernel of the 1.7 $M_\odot$ model in Fig. 7 remains much colder than the outer core. This is because the kernel is cooled by the powerful direct Urca process and thermal conduction is still unable to establish thermal relaxation throughout the core. Almost full core relaxation is achieved in 10 yr.

After the first year, the crust temperature profiles of the slow- and fast-cooling scenarios start to differ. In the former, the temperature gradient between the core and the crust is slowly eroded, as the cooling wave from the centre reaches the surface. In the latter, the temperature gradient continues to grow until it reaches a maximum at $t \sim 10$ yr. Then a huge amount of heat is released from the crust and leads to a spectacular drop in the surface temperature by an order of magnitude (which lowers the photon luminosity by four orders of magnitude). At $t = 50$ yr, the entire star is already isothermal. Note that, despite larger temperature gradients, thermal relaxation proceeds more quickly overall in the fast cooling scenario.

Prior to thermal relaxation, the contributions of the neutron star crust to the integrated heat capacity and neutrino luminosity are significant (Figs 8 and 9). In the slow-cooling models, the heat capacity in the crust ranges from 10 to 20 per cent of that in the core, with the larger fraction in the low-mass models (where crusts occupy a larger fraction of the volume). In the fast-cooling models, the ratio of the crust to core heat capacities reaches a maximum of 55 per cent at $t \sim 10$ yr before dropping to under 10 per cent after the relaxation. Similarly, the integrated neutrino luminosity of the crust is about 15–40 per cent of that of the core at $t \sim 1$ yr, and then it drops to a tiny fraction at later times.

The importance of the individual neutrino mechanisms for the crust cooling varies at different epochs. First, for $t < 10^{-2}$ yr in the fast-cooling scenario or for $t < 3 \times 10^{-3}$ yr in the slow-cooling scenario, the e^-e^+ pair emission controls the crust temperature. As the temperature drops below 5×10^9 K, this process quickly fades away. The next epoch is controlled by plasmon decay. It dominates for $10^{-2} < t \lesssim 10$ yr (fast cooling) or $3 \times 10^{-3} < t \lesssim 10$ yr (slow cooling). The last epoch of thermal relaxation lasts for a period of $10 \lesssim t < 100$ yr (fast cooling) or $10 \lesssim t < 1000$ yr (slow cooling), where either electron–nucleus or neutron–neutron bremsstrahlung is important. In fact, both neutrino processes give almost identical cooling curves in the absence of superfluidity. However, free neutrons in the crust are thought to be in a superfluid state which strongly suppresses nn bremsstrahlung. Therefore, electron–nucleus bremsstrahlung is likely to be the dominant neutrino mechanism in this last epoch.

4 RELAXATION TIME

The duration of the thermal relaxation epoch is potentially interesting from the observational point of view. This problem has been studied in a number of papers, with the most detailed and thorough work by Lattimer et al. (1994, and references therein). Those authors considered thermal relaxation for the fast cooling and defined the relaxation time t_w as the moment of the most negative slope of the cooling curve, $\ln T_s(\ln t)$, of a young neutron star. This is a typical time for the cooling wave to reach the surface.
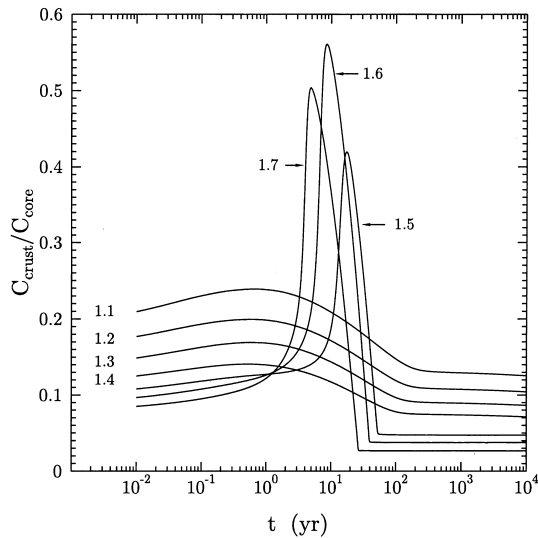
Figure 8. Ratio of the integrated heat capacities in the crust and the core for the neutron star models of masses 1.1, 1.2, ..., 1.7 M⊙.
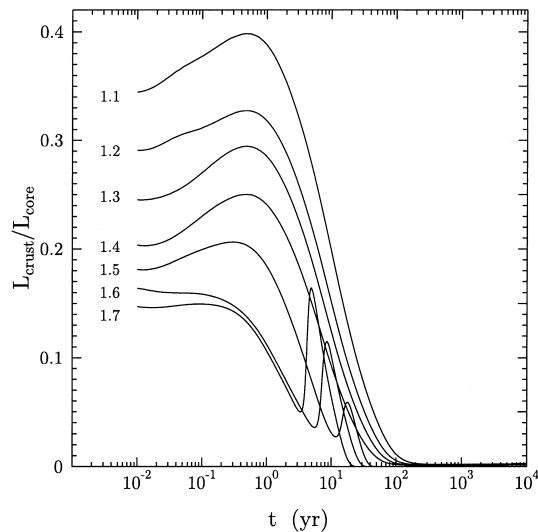

Figure 9. Ratio of the neutrino luminosities in the crust and the core for the neutron star models of masses 1.1, 1.2, ..., 1.7 M⊙.

We will focus mainly on the case of rapid cooling, where the relaxation effects are more pronounced.

According to Lattimer et al. (1994), the relaxation time of rapidly cooling neutron stars of various masses is determined mainly by the crust thickness ΔR_{crust} and is given by a simple scaling relation

$$t_w \approx \alpha \, t_1, \quad \alpha \equiv \left(\frac{\Delta R_{crust}}{1\,km}\right)^2 (1 - r_g/R)^{-3/2}. \qquad (3)$$

Here, t_1 is the normalized relaxation time which depends solely on the microscopic properties of matter, such as the thermal conductivity and heat capacity. In superfluid neutron stars, t_1 is sensitive to the magnitude and density dependence of the critical temperature of neutron superfluidity in the crust, as we discuss later. It is important that t_1 appears to be almost independent of the neutron star model, its mass M and radius R. We have verified that this scaling holds also for the slow-cooling non-superfluid models.
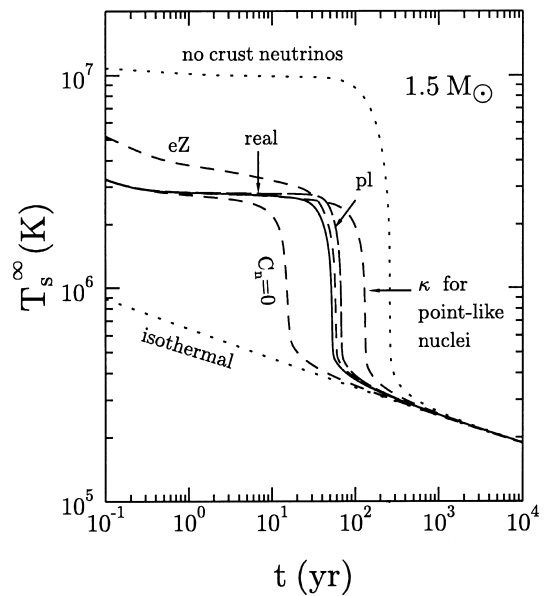

Figure 10. Thermal relaxation for the 1.5-M⊙ model without superfluid effects (see also Table 2). Solid line: cooling curve for the best values of the thermal conductivity, heat capacity, and neutrino emissivity. Dotted lines: switched-off neutrino emission from the crust (upper) or infinite thermal conductivity at $\rho > 10^{10}\,g\,cm^{-3}$ (lower). The dashed curve $C_n = 0$: removed neutron heat capacity in the crust. The dashed curve κ: the thermal conductivity in the crust for point-like nuclei. Two other dashed lines: removed all neutrino mechanisms in the crust except either plasmon decay (pl) or electron–nucleus bremsstrahlung (eZ).

For the non-superfluid stars with the core–crust interface placed at $\rho_0/2$, which is close to our value $\rho_{cc} = 1.5 \times 10^{14}\,g\,cm^{-3}$, Lattimer et al. (1994) obtained $t_1 \approx 26\,yr$. Our rapidly cooling models show similar scaling, $t_1 = 28.4 \pm 0.2\,yr$, whereas in the slowly cooling models $t_1 = 32.9 \pm 1.2\,yr$.

The dependence of t_w on the thermal conductivity κ and heat capacity C_v follows from a simple estimate of the thermal relaxation time in a uniform slab of width l:

$$t_w \sim C_v l^2/\kappa. \qquad (4)$$

The proper width of a thin crust ($\Delta R_{crust} \ll R$), taking into account the effects of general relativity, is $l = \Delta R_{crust}/\sqrt{1 - r_g/R}$. This gives $t_w \propto 1/(1 - r_g/R)$ in equation (3). An additional factor of $1/\sqrt{1 - r_g/R}$ accounts for the gravitational dilation of time intervals.

The parameter t_1 can be roughly estimated using equation (4) with the values of the specific heat capacity and thermal conductivity in the crust near the crust–core interface, for instance, at $\rho = 10^{14}\,g\,cm^{-3}$. Fig. 7 shows that the relevant temperature at the interface is $T \approx 2 \times 10^8\,K$. At those temperature and density values, according to our physics input, $C_v = 1.9 \times 10^{19}\,erg\,cm^{-3}\,K^{-1}$ and $\kappa = 1.8 \times 10^{20}\,erg\,cm^{-1}\,s^{-1}\,K^{-1}$. This gives $t_1 \sim (1\,km)^2 C_v/\kappa \approx 34\,yr$, which is in qualitative agreement with the model value.

Fig. 10 shows the sensitivity of the relaxation time to test variations of physical properties of the neutron star crust in the fast cooling scenario of the 1.5-M⊙ star. The corresponding values of t_w and t_1 are listed in Table 2. They may differ from the mean values (Table 3) within the error-bars. We present also the results for the superfluid models discussed in the next section. The solid ('real') curve is taken from Fig. 5. It is calculated using the best available physics input for a non-superfluid neutron star model.

Table 2. Relaxation time t_w and normalized time t_1 for neutron stars with different crust models.

Test crust model	t_w (yr)[a]	t_1 (yr)[a]	t_1 (yr)[b]
Real model, no SF	52.4	28.8	33.9
no crust neutrinos	253.5	139.2	134.9
only plasmon decay neutrinos	67.6	37.1	41.6
only eZ neutrino bremsstr.	58.3	32.0	34.5
no neutron heat capacity	15.3	8.4	6.7
cond. for point-like nuclei	131.8	72.4	102.3
Real model, weak crust SF	20.2	11.1	3.3
no Cooper neutrinos	29.0	15.9	19.0
weak core + crust SF	22.3	12.2	25.7
Real model, strong crust SF	15.0	8.2	6.7
no Cooper neutrinos	15.5	8.5	6.9
strong core + crust SF	10.7	5.9	5.8

[a] for the $1.5\,M_\odot$ model, with $\alpha = 1.821$.
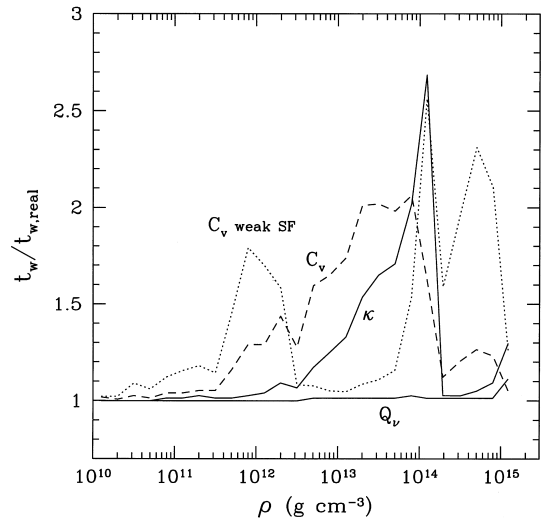[b] for the $1.3\,M_\odot$ model, with $\alpha = 2.875$.

Table 3. Normalized relaxation times in the crust t_1, equation (3), and in the core t_2, equation (5).

	Fast cooling	Slow cooling
Crust t_1 (yr)		
no SF	28.4 ± 0.2	32.9 ± 1.2
weak crust SF	10.3 ± 0.6	3.4 ± 0.3
weak core + crust SF	11.5 ± 0.5	25.0 ± 0.4
strong crust SF	7.0 ± 0.9	6.8 ± 1.0
strong core + crust SF	6.2 ± 0.4	5.7 ± 0.2
Core t_2 (yr)		
no SF	9.1 ± 0.8	
weak core SF	11.2 ± 0.5	
strong core SF	3.6 ± 0.2	

Switching off the neutrino emission from the crust, while keeping the heat capacity, slows down the thermalization epoch by almost an order of magnitude, from 50 to 250 yr. Turning on the plasmon decay alone would lead to the cooling curve not very different from the real one, although the thermalization epoch would be delayed by about 30 per cent ($t_w = 68$ yr). Turning off the plasmon decay and switching on the electron–nucleus bremsstrahlung instead would give a hotter neutron star before the relaxation but almost correct relaxation time, $t_w = 58$ yr. Combined together, plasmon decay and electron–nucleus bremsstrahlung would accurately reproduce the real cooling curve.

Restoring the neutrino emissivity in the crust but switching off the heat capacity of crustal neutrons ($C_n = 0$) we obtain much faster relaxation, which lasts about 15 yr. This numerical experiment imitates the suppression of the neutron heat capacity by strong neutron superfluidity (discussed in Section 5). On the other hand, had we neglected the quantum suppression of the heat capacity of the nuclei below the Debye temperature, the latter heat capacity would have become important in older neutron stars, $t \gtrsim 10^4$ yr, strongly delaying the cooling.

Finally, the relaxation time depends on the thermal conductivity in the inner crust. For instance, a neglect of the finite sizes of atomic nuclei in the electron–nucleus scattering rate would lower the electron thermal conductivity at the crust base ($\rho \gtrsim 10^{13}\,\mathrm{g\,cm^{-3}}$) by a factor of 2–5 (cf. Fig. 4). Using that less realistic thermal conductivity we would have had much longer relaxation (about 130 yr). If the thermal conductivity were infinite in the stellar interior (at $\rho > \rho_b$), we would have obtained an

Figure 11. Sensitivity of the crust relaxation time to the variations of the heat capacity, thermal conductivity, and neutrino emissivity in various density regions of the 1.5-$M_\odot$ neutron star model with the non-superfluid core. In each 0.2 dex of $\log \rho$, Q_ν and κ are reduced by a factor of 8 (solid lines, no superfluidity), and C_v is enhanced by a factor of 8 without superfluid effects (dashes) and with weak superfluidity (dots).

isothermal cooling scenario. In this case a sharp drop of the surface temperature associated with the relaxation disappears.

We have run additional cooling models with $M = 1.5\,M_\odot$, varying the heat capacity and thermal conductivity within the crust (at $\rho_b \leq \rho \leq \rho_{cc}$) by a fixed factor of 1/8, 1/4, 1/2, 2, 4 or 8. The results confirm that t_w and t_1 are indeed quite sensitive to the variations of C_v and κ, in agreement with the qualitative estimate, equation (4), and the results of Lattimer et al. (1994). It is important that these variations do not invalidate the scaling relation for the relaxation time; see equation (3). Moreover, if C_v is increased and κ is decreased, the dependence of t_1 on the values of the heat capacity and thermal conductivity is described by a simple scaling relation $t_1 \propto C_v/\kappa^{0.8}$.

We have also done sensitivity tests of the relaxation time, analogous to those performed by Epstein et al. (1983). In each density region, 0.2 dex of $\log \rho$, either the heat capacity, thermal conductivity, or neutrino emissivity have been changed by a factor 1/8, 1/4, 1/2, 2, 4 or 8. Fig. 11 shows the variations of t_w when Q_ν and κ are reduced by a factor of 8, and C_v is enhanced by a factor of 8. The relaxation time depends mostly on the values of C_v and κ in the crust in the density range 10^{13}–$1.5 \times 10^{14}\,\mathrm{g\,cm^{-3}}$ near the crust–core interface, being rather insensitive to the variations of Q_ν. Variations of the physical parameters in the core affect the crustal relaxation much less strongly (at least for non-superfluid models). The density range where t_w is most affected by the variations of κ is narrower than the density range where it is affected by the variations of C_v. The most important temperature range which influences t_w is $10^8 \lesssim T \lesssim 10^9$ K. The properties of matter in these 'sensitivity strips' of ρ and T are very model-dependent. For instance, the nuclei may be strongly non-spherical (rods, plates, etc.) at $\rho > 10^{14}\,\mathrm{g\,cm^{-3}}$, which is not included in our calculations. Note that the thermal conductivity has not been calculated so far for the phase of non-spherical nuclei.

However, if C_v were noticeably lower, or κ were noticeably higher than in our basic non-superfluid models, the decrease of the crust relaxation time would saturate at $t_w \approx 13$ yr. This is the time it takes the inner core with the direct Urca emission to equilibrate

thermally with the outer core (cf. Fig. 7). More generally, this is a core relaxation time t_{core}, which is almost independent of the parameters of the crust. It can be estimated using the same formalism of heat diffusion as in equation (4) through a slab of material between the direct-Urca-allowed kernel and the boundary of the core, with $l = R_{core} - R_D$. The relativistic factors appear as $(e^{-\Phi_{cc}})^3$, where Φ_{cc} is the metric function at the core–crust interface.

We have calculated the core relaxation time by setting the crust conductivity very high for the fast cooling models of non-superfluid neutron stars with $M = 1.5, 1.6, 1.7 \, M_\odot$. The least-squares fit gives

$$t_{core} = t_2 \left(\frac{R_{core} - R_D}{10 \, km} \right)^2 e^{-3\Phi_{cc}}, \tag{5}$$

with $t_2 = (9.1 \pm 0.8)$ yr. Thus, the fast-cooling models may have two distinct relaxation times, in the core and in the crust, and the latter is typically longer, at least for non-superfluid models.

The normalized crustal relaxation time t_1 shows very small variations with the neutron star mass, ± 0.2 yr for fast cooling and ± 1.2 yr for slow cooling (see Table 3). Even combining the models with all masses we find that the scaling relation, equation (3), holds remarkably well, and $t_1(all) = 31 \pm 2$ yr. Therefore, the cooling of the crust prior to thermal relaxation is indeed insensitive to the thermal evolution of the core. The slow cooling makes the relaxation much less pronounced but it does not change its basic features. This property is a result of the very high thermal conductivity in the core (Fig. 4), which makes the core-relaxation time typically much shorter than the crust one. Accordingly, the cooling curves do not depend on the exact value of the conductivity in the core as long as it is much higher than in the crust.

Among earlier works on thermal relaxation in young neutron stars we would like to also mention the papers by Nomoto & Tsuruta (1981, 1987). These authors used a different definition of t_w, defining it as the time when the real cooling curve differs by 0.5 per cent from the isothermal one. Naturally, this definition yields a longer t_w than the 'physical' relaxation time, during which departures from isothermality can be important. Thus, contrary to Nomoto and Tsuruta's conclusion, most neutron stars from the 10^3–10^4 yr old supernova remnants can be described quite accurately by isothermal models.

Nomoto & Tsuruta (1987) correctly noticed the dependence of the relaxation time on the equation of state for the fixed stellar mass of $1.4 \, M_\odot$: t_w is longer for the stiffer equation of state (with a thicker crust). This dependence was quantified later as equation (3) by Lattimer et al. (1994). Unfortunately, we cannot make a quantitative comparison with those earlier results because the physics input has changed significantly from the 1980s. Nomoto and Tsuruta also observed that superfluidity in the core and the crust plays an important role in regulating thermal relaxation. We consider the superfluid effects next.

5 EFFECTS OF SUPERFLUIDITY

Free neutrons in the crust and both neutrons and protons in the core of a neutron star are likely to be in the superfluid state. We implement the effects of superfluidity as discussed in Section 2.2. It turns out that superfluidity in the crust affects the cooling curves at the thermal relaxation stage, while superfluidity in the core affects cooling at later stages. First, consider the effects of neutron superfluidity in the crust. If the temperature T falls much below the
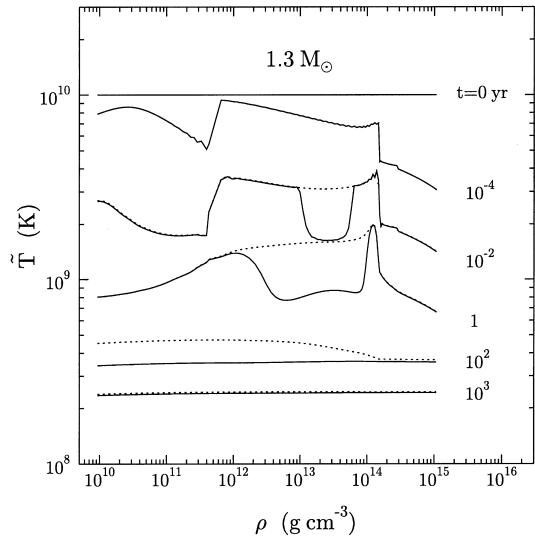

Figure 12. Temperature profiles in the interior of the $1.3 \, M_\odot$ model with (solid lines) and without (dots) weak crust superfluidity of free neutrons. The core is not superfluid. Numbers next to curves show the stellar age. The contours are at 0, 10^{-4}, 10^{-2}, 1, 100 and 1000 yr.

critical temperature T_{cn}, the superfluidity strongly reduces the neutron heat capacity and nn neutrino bremsstrahlung. While the latter is compensated by electron–nucleus bremsstrahlung, the former effect leads to a faster thermal relaxation. In addition, a new neutrino process is allowed in the superfluid state: the neutrino emission as a result of Cooper pairing of free neutrons. It further accelerates cooling and thermal relaxation of the crust.

Fig. 12 illustrates how the weak neutron superfluidity in the crust carves out the temperature profiles in the standard cooling scenario, $M = 1.3 \, M_\odot$. For the first 10^{-4} yr, when the temperature is above T_{cn}, the thermal structure is identical to that of the non-superfluid model. Later, the region where the critical temperatures are the highest cools much faster than the neighboring layers. The acceleration of cooling is mainly as a result of the reduction of the heat capacity and the switching on of the Cooper-pairing neutrino emission. A sequence of points in Fig. 12, in which solid lines start to deviate from the dotted ones, can reproduces the density profile of T_{cn} shown in Fig. 1. As the temperature falls further, wider density regions become affected, producing shells of cool matter surrounded on both sides by hotter layers. After the cooling wave from the core reaches the outer crust, the star settles into almost the same isothermal state as the non-superfluid model, but at a greater rate.

The effects are much stronger if the superfluidity is allowed for inside the stellar core. Fig. 13 shows the combined effect of the strong superfluidity in the core and crust. Both neutrons and protons are superfluid in the core of this 1.5-$M_\odot$ neutron star. In addition to the trough in the crust layers, the core develops a complex structure. All the sources of neutrino emission and the nucleon heat capacity in the core are affected by the superfluidity, while the electron heat capacity is not and becomes dominant in highly superfluid cores. As soon as the temperature drops significantly below the critical temperatures T_{cn} or T_{cp}, Cooper-pairing neutrino emission comes into play. It starts in the inner part of the core and drives the temperature down. At $t \sim 10^{-2}$ yr that region is even cooler than in the non-superfluid model, while the other parts of the core are slightly hotter. By the age of 1 yr, this cool region includes all of the core except the inner kernel. As a
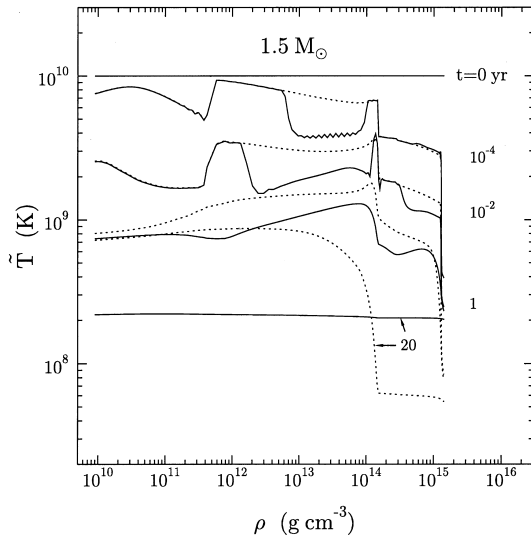
Figure 13. Temperature profiles (solid lines) in the interior of the 1.5-$M_\odot$ model with strong superfluidity both in the crust and the core. The numbers next to the curves show the stellar age. The contours are at 0, 10^{-4}, 10^{-2}, 1 and 20 yr. The dotted lines show the temperature profiles of the non-superfluid star.
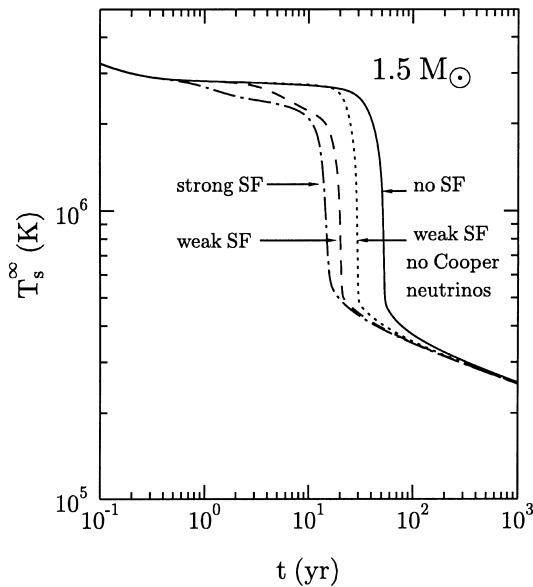

Figure 14. Superfluid effects in the crust of the 1.5-$M_\odot$ neutron star model with the non-superfluid core. The dashed line is for the case of weak neutron superfluidity, while the dash-and-dot line is for the case of strong superfluidity. The dotted line is obtained neglecting the Cooper-pair neutrino emission for the weak-superfluid model. The solid line is the cooling curve for the non-superfluid crust.

result, thermal relaxation proceeds on a shorter time-scale, and at $t \lesssim 20\,\mathrm{yr}$ the stellar interior is isothermal. Thus, for the large assumed values of T_{cn} and T_{cp} the neutrino emission caused by Cooper pairing becomes so strong that, instead of slowing down, the presence of the core superfluidity accelerates the cooling.

Fig. 14 demonstrates the aforementioned effects on the thermal relaxation time in the 1.5-$M_\odot$ neutron star. The stellar core is assumed to be non-superfluid. The thermal relaxation stage occurs about 2.6 times faster in the case of weak crust superfluidity and

about 3.5 times faster in the case of strong crust superfluidity, compared to the non-superfluid crust. And also, while the inclusion of the neutrino emission caused by Cooper pairing leads to faster cooling for $t < 20\,\mathrm{yr}$, most of the accelerating effect is a result of the reduction of the crust heat capacity. Therefore, the *relaxation time is greatly reduced by the effect of superfluidity on the heat capacity of free neutrons in the stellar crust.*

Still, the relaxation time of the superfluid crust satisfies the same scaling relation, equation (3), as for the non-superfluid crust. Table 3 summarizes the results, taken as the mean of $M = 1.5$, 1.6, and 1.7-$M_\odot$ models for fast cooling, and $M = 1.1$, 1.2, 1.3, and 1.4-$M_\odot$ models for slow cooling. In case of the fast-cooling models, crust superfluidity reduces the relaxation time by up to a factor of four; $t_1 = 7.0 \pm 0.9\,\mathrm{yr}$ for the strong superfluidity. In case of the slow-cooling models with strong crust superfluidity the effect is similar, but with the weak superfluidity it is much different, by almost a factor of 10. The inclusion of superfluidity in the core does not affect the relaxation time significantly. The values of t_1 change by about $\approx 1\,\mathrm{yr}$ and are within the error-bars of the results for the non-superfluid cores. Again the notable exception is the weak superfluidity in the slow-cooling models.

Superfluidity in the core changes the core relaxation time, although it still scales as in equation (5). Weak core superfluidity only increases the core heat capacity and delays the relaxation by a few years, $t_2 = 11.2 \pm 0.5\,\mathrm{yr}$, while the strong superfluidity suppresses the heat capacity and gives much faster relaxation, by a factor of 2.5.

The large difference of the values of t_1 for the slowly and rapidly cooling stars with weakly superfluid crusts indicates that, generally, superfluidity may violate the simple scaling relations for the relaxation time as well as the strict thermal decoupling of the crust and the core prior to the relaxation. This happens because superfluidity makes the heat capacity (and other properties of matter) a strong function of density.

The shortening of the thermal relaxation phase in a rapidly cooling star, as a result of the superfluid reduction of the crustal heat capacity, was emphasized by Lattimer et al. (1994). Using a model of superfluidity, which is closer to our model of strong superfluidity in the crust, Lattimer et al. found that the relaxation time becomes three times as short, $t_w = 8.4 \pm 2.0\,\mathrm{yr}$, in qualitative agreement with our results. Our calculations indicate that the effect is sensitive to the model of neutron superfluidity in the crust and thus it can be used to test such models.

When thermal relaxation is over, the cooling is mainly regulated by the neutrino luminosity and heat capacity of the core. The processes in the crust cease to play a significant role except for the very low-mass neutron stars with large crusts. We find, however, that for some superfluid models the neutrino luminosity of the crust may affect the cooling for a short period of time during the transition from the neutrino cooling era to the photon era. For instance, cooling of superfluid neutron stars after the thermal relaxation is discussed in detail by Yakovlev et al. (1999).

6 CONCLUSIONS

We have studied thermal evolution of young neutron stars using a new cooling code and updated physics input. The effective surface temperature of isolated neutron stars in the first 100 yr is determined by the properties of the crust. After the cooling wave from the core reaches the surface, the effective temperature drops from 250 eV to 50 eV or lower. We confirm the conclusion of Lattimer et al. (1994) that the duration of the relaxation epoch in a

fast cooling scenario depends sensitively on the heat capacity and thermal conductivity of the crust. The relaxation time scales with the size of the crust, equation (3), and the normalization is $t_1 = 28$ yr without superfluid effects or $t_1 = 7$ yr with strong superfluid effects. We find that the same conclusion holds in the case of slow cooling, in which thermal relaxation is less pronounced.

We also investigate the effects of various neutrino emission mechanisms in the crust, superfluidity of free neutrons, heat capacity, and thermal conductivity on the relaxation time (as summarized in Table 2 and Fig. 11). The relaxation time is most sensitive to the variations of κ and C_v in the density range 10^{13}–1.5×10^{14} g cm^{-3} near the crust–core interface.

Young cooling neutron stars can serve as astrophysical laboratories of matter at subnuclear densities. The sensitive dependence of the relaxation time on the microscopic properties of matter in the deep inner crust provides a possibility to study these properties by observing the emergence of the cooling wave. In order to realize this method, one needs to detect thermal emission from a very young neutron star in the range from 50 to 250 eV. Such stars have not been found so far, but may be detected in young supernova remnants by *Chandra* and *XMM*.

To improve the cooling theory of young neutron stars, it would be desirable to continue theoretical studies of microscopic properties of matter in the inner crust, in particular, the possible unusual phases of nonspherical nuclei at $\rho > 10^{14}$ g cm^{-3}, as well as the thermal conductivity, heat capacity and neutrino emission of such matter. The evolution of a possible magnetic field in the crust needs to be addressed, as a strong field may alter the electron conductivity and other transport phenomena. It is also important to refine our knowledge of matter containing spherical nuclei at $\rho \lesssim 10^{14}$ g cm^{-3}. In this paper (see the Appendix) we present and use the results of new calculations of the electron thermal conductivity determined by the scattering of electrons off spherical atomic nuclei, taking into account the effects of finite sizes and smoothed shapes of proton nucleus cores.

REFERENCES

Amundsen L., Østgaard E., 1985, Nucl. Phys. A, 442, 163
Baiko D. A., Potekhin A. Y., Kaminker A. D., Yakovlev D. G., 1998, Phys. Rev. Lett., 81, 5556
Baiko D. A., Haensel P., Yakovlev D. G., 2001, Nucl. Phys., in press (astro-ph/0105105)
Elgarøy Ø., Engvik L., Hjorth-Jensen M., Osnes E., 1996, Nucl. Phys. A, 604, 466
Epstein R. I., Gudmundsson E. H., Pethick C. J., 1983, MNRAS, 204, 471
Gnedin O. Y., Yakovlev D. G., 1995, Nucl. Phys. A, 582, 697
Gudmundsson E. H., Pethick C. J., Epstein R. I., 1983, ApJ, 272, 286
Hoffberg M., Glassgold A. E., Richardson R. W., Ruderman M., 1970, Phys. Rev. Lett., 24, 775
Kaminker A. D., Pethick C. J., Potekhin A. Y., Thorsson V., Yakovlev D. G., 1999, A&A, 343, 1009
Kippenhahn R., Weigert A., Hofmeister E., 1967, Meth. Comput. Phys., 7, 129
Kittel C., 1986, Introduction to Solid State Physics. Wiley, New York
Lattimer J., Prakash M., 2000, ApJ, 550, 426
Lattimer J. M., Pethick C. J., Prakash M., Haensel P., 1991, Phys. Rev. Lett., 66, 2701
Lattimer J. M., Van Riper K. A., Prakash M., Prakash M., 1994, ApJ, 425, 802
Levenfish K. P., Yakovlev D. G., 1994, Astron. Zh., 71, 282 (English translation in Astron. Rep., 38, 247)
Lorenz C. P., Ravenhall D. G., Pethick C. J., 1993, Phys. Rev. Lett., 70, 379
Negele J. W., Vautherin D., 1973, Nucl. Phys. A, 207, 298
Nomoto K., Tsuruta S., 1981, ApJ, 250, L19
Nomoto K., Tsuruta S., 1987, ApJ, 312, 711
Oyamatsu K., 1993, Nucl. Phys. A, 561, 431
Page D., 1998a, in Buccheri R., van Paradijs J., Alpar M. A., eds, The Many Faces of Neutron Stars. Kluwer, Dordrecht, p. 539
Page D., 1998b, in Shibazaki N., Kawai N., Shibata S., Kifune T., eds, Neutron Stars and Pulsars. Universal Academy Press, Tokyo, p. 183
Page D., Applegate J. H., 1992, ApJ, 394, L17
Pethick C. J., 1992, Rev. Mod. Phys., 64, 1133
Pethick C. J., Ravenhall D. G., 1995, Ann. Rev. Nucl. Particle Sci., 45, 429
Potekhin A. Y., Baiko D. A., Haensel P., Yakovlev D. G., 1999, A&A, 346, 345
Potekhin A. Y., Chabrier G., Yakovlev D. G., 1997, A&A, 323, 415
Prakash M., Ainsworth T. L., Lattimer J. M., 1988, Phys. Rev. Lett., 61, 2518
Raikh M. E., Yakovlev D. G., 1982, Ap&SS, 87, 193
Shapiro S. L., Teukolsky S. A., 1983, Black Holes, White Dwarfs and Neutron Stars. Wiley-Interscience, New York
Thorne K. S., 1977, ApJ, 212, 825
Wambach J., Ainsworth T. L., Pines D., 1993, Nucl. Phys. A, 555, 128
Yakovlev D. G., 1987, SvA, 31, 347
Yakovlev D. G., Levenfish K. P., 1995, A&A, 297, 717
Yakovlev D. G., Levenfish K. P., Shibanov Yu. A., 1999, Uspekhi Fiz. Nauk, 169, 825 (English translation in Physics–Uspekhi 42, 737)
Yakovlev D. G., Gnedin O. Y., Potekhin A. Y., 2001a, Contrib. Plasma Phys., 41, 227
Yakovlev D. G., Kaminker A. D., Gnedin O. Y., Haensel P., 2001b, Phys. Rep., in press
Ziman J. M., 1960, Electrons and Phonons. Oxford Univ. Press, Oxford

APPENDIX A: ELECTRON CONDUCTIVITY OF THE INNER CRUST

In the inner crust, the electrons are strongly degenerate. The heat and charge are transported mainly by the electrons with energies in a narrow thermal band near the Fermi level ϵ_F. The coefficients of the electrical and thermal conductivities can be written as

$$\sigma = \frac{e^2 n_e \tau_\sigma}{m_e^*}, \quad \kappa = \frac{\pi^2 k_B^2 T n_e \tau_\kappa}{3 m_e^*}, \tag{A1}$$

where $m_e^* \equiv \epsilon_F / c^2$, n_e is the electron number density, k_B is the Boltzmann constant and τ_σ and τ_κ are the effective relaxation times. In the presence of several electron scattering mechanisms, the cumulative relaxation time is determined by the Matthiessen rule (e.g. Ziman 1960). In the envelopes of neutron stars, one traditionally considers the electron–ion (ei), electron–electron, and electron–impurity scatterings. We focus on the main mechanism, the ei scattering, which is electron scattering off strongly correlated ions – atomic nuclei – (if they form a Coulomb liquid) as well as scattering off ions which oscillate around their equilibrium positions (in a Coulomb solid). In the latter case, the adequate quantum-mechanical description is provided by the *electron–phonon* scattering formalism – cf. Baiko et al. (1998).

A modern theoretical treatment of the conductivities due to the ei scattering in strongly coupled Coulomb plasmas of ions has been

proposed by Baiko et al. (1998) and applied to the outer envelopes of neutron stars by Potekhin et al. (1999). In the latter work, practical formulae for σ and κ incorporating all three scattering mechanisms have been derived; the corresponding FORTRAN code is available electronically at http://www.ioffe.rssi.ru/astro/conduct/.

For the inner crust these expressions must be modified. First, the atomic nuclei cannot be considered as point-like. Secondly, the ei scattering in the inner crust at temperatures much below 10^8 K changes its character: so-called *umklapp* processes cease to dominate and the *normal* processes (with electron-momentum transfer within one Brillouin zone) become more important.

A1 Effects of the finite size of ions

The effective ei relaxation time is

$$\tau_{ei} = \frac{3\pi\hbar}{4Z\epsilon_F\alpha_f^2\Lambda_{ei}(\epsilon_F)}, \tag{A2}$$

where $\alpha_f \equiv e^2/(\hbar c)$ is the fine-structure constant, and Λ_{ei} is the Coulomb logarithm. For a classical plasma of ions in the Born approximation (e.g. Potekhin et al. 1999),

$$\Lambda_{ei} = \int_0^{2k_F} dq\; q^3|\phi(q)|^2 S(q)\left[1 - \beta_r^2\left(\frac{q}{2k_F}\right)^2\right], \tag{A3}$$

$$\phi(q) \equiv \frac{F(q)}{q^2\varepsilon(q)},$$

where $k_F = (3\pi^2 n_e)^{1/3}$ is the electron Fermi wave number, $\beta_r = v_F/c$, $v_F = \hbar k_F/m_e^*$ is the Fermi velocity, $\varepsilon(q)$ is the static dielectric function, $S(q)$ is the static structure factor of the ions (more precisely, its inelastic part – see Baiko et al. 1998) and $F(q)$ is the form factor of the ions. The latter three functions allow for the electron polarization, ion–ion correlations, and the finite size of the ions, respectively.

The quantization of ionic motion becomes important at $T \ll T_p$, where $T_p = \hbar\sqrt{4\pi n_i Z^2 e^2/M}/k_B$ is the ion plasma temperature, $n_i = n_e/Z$ is the ion number density, $M = Am_u$ is the ion mass, and m_u is the atomic mass unit. In this case, in equation (A3) one should use an *effective* structure factor, different for σ and κ. These effective factors have been derived by Baiko et al. (1998) and fitted by Potekhin et al. (1999) for the case where the umklapp processes dominate.

A1.1 Uniform charge distribution in atomic nuclei

At $\rho \ll \rho_{cc}$, a good approximation for the charge density within a nucleus is a step function. The corresponding form factor is

$$F(q) = \frac{3}{(qr_{nuc})^3}[\sin(qr_{nuc}) - qr_{nuc}\cos(qr_{nuc})], \tag{A4}$$

where r_{nuc} is the proton core radius.

In general, Λ_{ei} depends on ρ, T, Z, A and r_{nuc}, and it appears to be almost independent of the type of Coulomb lattice. It is convenient, however, to introduce dimensionless parameters: the electron relativity parameter $x_r = \hbar k_F/(m_e c)$; the ion size parameter $x_{nuc} = r_{nuc}/a_i$, where $a_i = (4\pi n_i/3)^{-1/3}$ is the ion-sphere radius; the Coulomb coupling parameter of ions $\Gamma = Z^2 e^2/(a_i k_B T)$; the inverse ion quantum parameter $t_p \equiv T/T_p$ and the electron screening parameter $s_e = k_{TF}^2/(2k_F)^2 = \alpha_f/(\pi\beta_r)$, where k_{TF} is the electron screening wave number. In accordance with the previous results, it is also convenient to introduce an auxiliary parameter

$s_D = (2k_F r_D)^{-2}$, where $r_D = a_i/\sqrt{3\Gamma}$ is the Debye screening length for the ideal plasma of ions. Finally, the basic parameters that characterize the Coulomb lattice are the normalized first- and second-negative moments of the phonon frequency, $u_{-1} \approx 3$ and $u_{-2} \approx 13$.

We have numerically calculated the effective Coulomb logarithms $\Lambda_{ei}^{\sigma,\kappa}$ for approximately 100 pairs (ρ, T), varying over orders of magnitude in the domain of strongly degenerate electrons and strongly coupled ions, for eight ion species from $(Z = 12$ to $Z = 60)$, and for five values of x_{nuc} (from 0 to 0.4). We have included the non-Born corrections in the same manner as Yakovlev (1987). The results can be fitted using the *effective screening function*

$$|\phi^{eff}(q)|^2 = \frac{1}{(q^2 + q_s^2)^2}[1 - e^{-s_0 q^2}]e^{-s_1 q^2}G_{\sigma,\kappa}D \tag{A5}$$

instead of $|\phi(q)|^2 S(q)$ in equation (A3). Here, the first term corresponds to the Debye screening with the effective screening wave number q_s, the factor in square brackets corrects for the ion correlations, and the functions G and D describe ionic quantum effects, as in Potekhin et al. (1999). An additional factor $e^{-s_1 q^2}$ plays a role of the effective form factor. The numerical values of Λ obtained from the accurate theory are reproduced (within several per cent in the most important ρ–T range) if we use the effective screening function (A5) with the following parameters:

$$s \equiv q_s^2/(2k_F)^2 = (s_i + s_e)e^{-\beta_Z}, \tag{A6}$$

$$\beta_Z = \pi\alpha_f Z\beta_r, \qquad s_i = s_D(1 + 0.06\Gamma)e^{-\sqrt{\Gamma}}; \tag{}$$

$$w \equiv (2k_F)^2 s_0 = (u_{-2}/s_D)(1 + \beta_Z/3); \tag{A7}$$

$$w_1 \equiv (2k_F)^2 s_0 = 14.73\, x_{nuc}^2(1 + \sqrt{x_{nuc}}\, Z/13)(1 + \beta_Z/3), \tag{A8}$$

$$G_\sigma = (1 + 0.0361 Z^{-1/3}t_p^2)^{-1/2}(1 + 0.122\beta_Z^2), \tag{A9}$$

$$G_\kappa = G_\sigma + \frac{0.0105 t_p}{(t_p^2 + 0.0081)^{3/2}}[1 + \beta_r^3\beta_Z](1 - Z^{-1})(1 + x_{nuc}^2\sqrt{2Z}), \tag{A10}$$

$$D = \exp\left[-0.42\sqrt{x_r/(AZ)}u_{-1}\exp(-9.1t_p)\right]. \tag{A11}$$

If $x_{nuc} = 0$, these equations reduce to those presented in Potekhin et al. (1999).

With the effective screening function in the form (A5), we can integrate equation (A3) analytically and obtain

$$\Lambda_{ei}^{\sigma,\kappa} = [\Lambda_0(s, w + w_1) - \Lambda_0(s, w_1)]G_{\sigma,\kappa}D, \tag{A12}$$

where

$$\Lambda_0(s, w) = \Lambda_1(s, w) - \beta_r^2\Lambda_2(s, w), \tag{A13}$$

$$2\Lambda_1(s, w) = \ln\frac{s + 1}{s} + \frac{s}{s + 1}(1 - e^{-w}) - (1 + sw)e^{sw}$$
$$\times [E_1(sw) - E_1(sw + w)], \tag{A14}$$

$$2\Lambda_2(s, w) = \frac{e^{-w} - 1 + w}{w} - \frac{s^2}{s + 1}(1 - e^{-w}) - 2s\ln\frac{s + 1}{s}$$
$$+ s(2 + sw)e^{sw}[E_1(sw) - E_1(sw + w)], \tag{A15}$$

and $E_1(x) = \int_x^\infty y^{-1}e^{-y}\,dy$ is the standard exponential integral. Note that using equations (A14) and (A15) directly may result in large numerical round-off errors in the limiting cases $s \ll 1$, $w \ll 1$, or $w \gg 1$. In these cases, explicit asymptotic expressions of Potekhin et al. (1999) should be used.

A1.2 Realistic charge distribution

Near the bottom of the crust, the boundary of the proton core in nuclei becomes fuzzy and the above results should be modified. Oyamatsu (1993) approximated the proton charge distribution by a function proportional to $(1 - r/r_\mathrm{m})^b$ (at $r < r_\mathrm{m}$), where the power index b controls the 'sharpness' of the charge profile. The parameters b and r_m have been described by the simple functions of mass density in the smooth composition model of crust matter (Kaminker et al. 1999). Using that model we have calculated the electrical and thermal conductivities for $\rho = 10^9 - 10^{14.1}\,\mathrm{g\,cm^{-3}}$ and $T = 10^7 - 10^9\,\mathrm{K}$, and compared the results with the fitting formulae (A12–A15). We have found that the electrical conductivity is reproduced (within ≈ 5–10 per cent), if we define x_nuc in equation (A8) so as to reproduce the same *mean-square* proton-core radius as in the approximation of uniform charge distribution:

$$x_\mathrm{nuc} = \frac{r_\mathrm{m}}{a_\mathrm{i}} \frac{1 - 15/(5 + b) + 15/(5 + 2b) - 5/(5 + 3b)}{1 - 9/(3 + b) + 9/(3 + 2b) - 1/(1 + b)}. \qquad \text{(A16)}$$

In equation (A10), which determines the thermal conductivity at $T \ll T_\mathrm{p}$, one should additionally multiply x_nuc by a factor of $b/(0.5 + b)$. The maximum-fit error of κ does not exceed 13 per cent.

A2 Normal processes at very low temperatures

Near the boundaries of the Brillouin zones the dispersion relation of electrons differs from the free-electron case, and at the boundaries the electron energy spectrum contains gaps. The gaps $\Delta\epsilon$ can be estimated in the weak coupling approximation (e.g. Kittel 1986) as $\Delta\epsilon \sim \phi(k_\mathrm{F}) = 4\pi Z e^2 n_\mathrm{i} k_\mathrm{F}^{-2} = 4e^2/(3\pi k_\mathrm{F})$. The effect of gaps is most significant if the deviation of the electron momentum from the intersection line between the Fermi surface and the Brillouin zone boundary does not exceed $\Delta k \sim \Delta\epsilon/(\hbar v_\mathrm{F}) \sim 4/3\pi(\alpha_\mathrm{f}/\beta_\mathrm{r})k_\mathrm{F} \ll k_\mathrm{F}$. However, with decreasing temperature the strips of the Fermi surface, between which the umklapps proceed effectively, become narrower and closer to these intersection lines. When the widths of the strips $[\sim t_\mathrm{p}(6\pi^2 n_\mathrm{i})^{1/3}]$ become smaller than Δk, the umklapp processes are frozen out and the normal processes prevail. The above estimates indicate that this happens when the temperature falls below

$$T_\mathrm{u} \sim T_\mathrm{p} Z^{1/3} \alpha_\mathrm{f}/(3\beta_\mathrm{r}). \qquad \text{(A17)}$$

In this case, the formalism used in Section A1 becomes invalid. The asymptotes for the ei scattering rates at $T \ll T_\mathrm{u}$ have been obtained by Raikh & Yakovlev (1982). In our notation, they yield

$$\left\{ \begin{array}{c} \Lambda_\mathrm{ei}^\sigma \\ \Lambda_\mathrm{ei}^\kappa \end{array} \right\} = \frac{a_\zeta x_\mathrm{r}^{1/2}}{A^{1/2} Z} \times \left\{ \begin{array}{c} (4/3)(\alpha_\mathrm{f}/\beta_\mathrm{r})t_\mathrm{p}^5 \\ \\ t_\mathrm{p}^3 \end{array} \right\}, \qquad \text{(A18)}$$
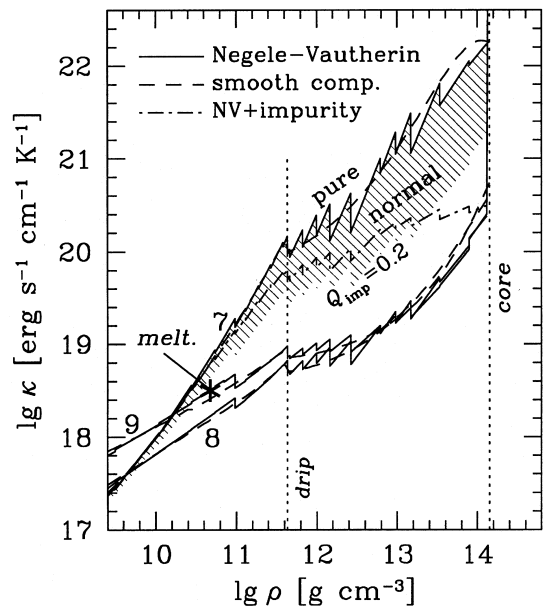

Figure A1. Density dependence of the electron thermal conductivity at $T = 10^7$, 10^8 and $10^9\,\mathrm{K}$ in the neutron star crust. Solid and dot-dashed lines: ground state composition (Negele & Vautherin 1973), rectangular profile of nuclear charge (solid lines: pure crystal or liquid; dot-dashed line: including impurities; bottom of the hatched region: neglecting freezing of umklapp processes at $T = 10^7\,\mathrm{K}$); dashed lines: smooth-composition model, realistic profile of nuclear charge, no impurities.

where

$$a_\zeta = 180 \left(\frac{3}{\pi \alpha_\mathrm{f}} \frac{m_\mathrm{e}}{m_\mathrm{u}} \right)^{1/2} \zeta(5) \approx 50,$$

and $\zeta(5) = 1.0369$ is the value of the Riemann zeta function.

Now we interpolate between the high-temperature Coulomb logarithm $\Lambda_\mathrm{ei,high}^{\sigma,\kappa}$ given by equation (A12) and the low-temperature asymptote $\Lambda_\mathrm{ei,low}^{\sigma,\kappa}$ given by equation (A18):

$$\Lambda_\mathrm{ei}^{\sigma,\kappa} = \Lambda_\mathrm{ei,high}^{\sigma,\kappa} \exp(-T_\mathrm{u}/T) + \Lambda_\mathrm{ei,low}^{\sigma,\kappa}[1 - \exp(-T_\mathrm{u}/T)]. \qquad \text{(A19)}$$

Fig. A1 shows the thermal conductivities for three values of the temperature. In the neutron star envelope, the plasma is in the solid phase except for the segment to the left of the asterisk at the highest $T = 10^9\,\mathrm{K}$. At the lowest $T = 10^7\,\mathrm{K}$, the change in the scattering from umklapp to normal processes leads to a significant increase in the conductivity shown by the hatched region. However, this increase can be compensated by the scattering off impurities. For example, the dashed line shows the conductivity for $Q_\mathrm{imp} \equiv \langle (Z_\mathrm{imp} - Z)^2 n_\mathrm{imp} \rangle / n_\mathrm{i} = 0.2$, where n_imp and Z_imp are the impurity number density and charge number, respectively. For comparison, dashed lines show the thermal conductivity in the smooth-composition model with smooth proton charge profile.